Bulletin of Geophysics and Oceanography Vol. XX, n. X, pp. XXX-XXX; Xxxxx 20xx
DOI 10.4430/bgo00513

Assessment of minimum entropy velocity analysis

E. Ligas[1], N. Bienati[2] and M. Pipan[1]

[1] *University of Trieste, Italy*
[2] *Eni Natural Resources, Milano, Italy*

(Received: 26 June 2025; accepted: 8 November 2025; published online: 20 February 2026)

ABSTRACT The shift to renewable energy has heightened the demand for efficient, cost-effective subsurface imaging, especially for offshore wind farms and underground storage of carbon or hydrogen. These projects frequently depend on short-offset or single-channel seismic data due to logistical and financial constraints, which restrict the resolution of traditional velocity analysis. This work presents a novel method to improve seismic imaging from post-stack data by integrating image focusing into full-waveform inversion (FWI). We include minimum entropy velocity analysis as a cost function within FWI, evaluating subsurface models based on the focusing quality of reverse time migration images using the minimum entropy (ME) norm. Validation on a synthetic dataset shows that, although the ME-norm itself can be ambiguous, its derivative reliably indicates the correct velocity. This insight leads to a new cost function whose gradient, computed via the adjoint-state method, effectively guides model updates through the steepest-descent method. Application to a marine dataset from the Viking Graben (North Sea) demonstrates enhanced image quality, with better reflector alignment and contrast. These results highlight the potential of ME-norm derivatives to drive FWI, thus enabling advanced velocity model building from short-offset or single-fold data with lower computational costs.

Key words: seismic reflection, imaging, small offset, velocity analysis, focusing.

1. Introduction

The global shift towards renewable energy is expanding the use of geophysical subsurface prospecting into new application domains, including the characterisation of offshore wind farm sites and the monitoring of geological storage for carbon dioxide and hydrogen. These emerging applications often demand repeated surveys and high-resolution subsurface imaging, making data acquisition a significant logistical and financial challenge. To remain feasible and cost-effective, many projects rely on single-channel systems or short-offset multichannel seismic cables: an approach also common in academic marine geophysics, where seismic datasets are typically acquired under tight constraints.

While these acquisition strategies provide practical benefits, they inherently lack the offset diversity required for conventional moveout-based velocity analysis (Nasif, 2024). Accurate depth-domain velocity models are crucial for a quantitative interpretation beyond time-migrated images, which are often insufficient for evaluating formation thickness, fault dip, or true structural geometry. Therefore, there is an urgent requirement for advanced methods that can produce reliable depth velocity models from limited-offset seismic data, thereby enhancing the interpretability of subsurface features in data-constrained environments.

This work presents a novel approach to velocity analysis for depth imaging that leverages subsurface imaging, focused on addressing the limitations of short-offset seismic data. Specifically, the research aims to adapt full-waveform inversion (FWI) to post-stack seismic data, using a cost function based on image focusing rather than the conventional misfit between modelled and observed data. The proposed approach is expected to be computationally more efficient because it operates on post-stack data, thereby reducing both computational costs and data requirements. This makes advanced imaging techniques more accessible across a broader range of applications.

By concentrating on image sharpness, this technique aims to improve the resolution and accuracy of subsurface images, which is crucial for applications requiring precise geological and geophysical interpretations. However, it is important to recognise that the effectiveness of this approach depends on the presence of diffractions in the data; in environments dominated by flat, laterally continuous layers, the use of this technique is limited in its applicability.

Previous work on velocity analysis based on image focusing can be found in De Vries and Berkhout (1984), in which they described minimum entropy velocity analysis (MEVA) as a procedure to extract velocity information from the focusing of diffraction energy. Another significant contribution by Biondi (2010) introduces a method for estimating migration velocity from seismic data by analysing the focusing and defocusing of residual-migrated images. Also, the work by Weibull and Arntsen (2014) introduces reverse time demigration methods to improve velocity models and enhance seismic imaging accuracy, especially for complex geological media. Santos *et al*. (2020) applied diffraction velocity analysis to single-channel seismic data from the Joetsu basin, showing that diffraction-based velocity extraction improves imaging in data-sparse environments. Fomel *et al*. (2007) developed a post-stack diffraction velocity analysis using a local varimax focusing measure, conceptually similar to our formulation of the minimum entropy (ME) norm, with which they achieved efficient velocity updates without full pre-stack modelling. Also, Preine *et al*. (2020) used diffraction-based wavefront tomography in the Santorini–Amorgos tectonic zone, employing diffraction focusing as a quality-control tool to derive depth-velocity models consistent with geological structures.

2. Methods

This research builds on the work of De Vries and Berkhout (1984), primarily aiming to integrate MEVA into the FWI framework.

The proposed method estimates the focusing quality of seismic images produced by post-stack reverse time migration (RTM) (Baysal *et al*., 1983; Whitmore, 1983), based on the assumption, originally introduced by De Vries and Berkhout (1984) that the optimal velocity model corresponds to the best-focused image, as measured by the ME norm.

The main goal is to reformulate MEVA as a cost function within the FWI algorithm to update an initial velocity model. To this end, RTM was used to generate migrated images using different test velocities, and assess their focusing through the ME norm, ultimately leading to the definition of a new cost function.

2.1. Minimum entropy norm

Following De Vries and Berkhout (1984) we define the ME norm based on a migrated seismic image composed of $N = N_1 \times N_2$ samples $p_{k,l}$ with $k = 0, \ldots, N_1\text{-}1$ and $l = 0, \ldots, N_2\text{-}1$. At first, the

positive parameter $a'_{k,l}$ is defined as:

$$a'_{k,l} = \frac{a_{k,l}}{\sum_{k=0}^{N_1-1}\sum_{l=0}^{N_2-1} a_{k,l}} \tag{1}$$

that is the amplitude of the $(k,l)^{th}$ sample ($a_{k,l} = p^2_{k,l}$) normalised over the sum of the amplitude distribution. A scale-independent version of the amplitude could be defined as:

$$q_{k,l} = N a'_{k,l} = \frac{a_{k,l}}{\frac{1}{N}\sum_{k,l} a_{k,l}}. \tag{2}$$

Since the acoustic energy is proportional to the square of the pressure divided by the square of the velocity $E \propto p^2/c^2$, the pressure field by the velocity model was scaled, thus obtaining:

$$q_{k,l} = \frac{\left(p_{k,l}/c_{k,l}\right)^2}{\frac{1}{N}\sum_{k,l}\left(p_{k,l}/c_{k,l}\right)^2}. \tag{3}$$

According to De Vries and Berkhout (1984), a measure of the image resolution could be computed by the ME norm defined as:

$$ME = \frac{1}{N}\sum_{k=0}^{N_1-1}\sum_{l=0}^{N_2-1} q_{k,l} F(q_{k,l}) \tag{4}$$

where the entropy function $F(q_{k,l})$ is a monotonically increasing function of $q_{k,l}$ used as a measure of resolving power. A simple choice is $F(q_{k,l}) = q_{k,l}$ which gives:

$$ME = \frac{1}{N}\sum_{k,l} q_{k,l} q_{k,l} = N \sum_{k,l} \frac{\left(p_{k,l}/c_{k,l}\right)^4}{\left(\sum_{m,n}\left(p_{m,n}/c_{m,n}\right)^2\right)^2}. \tag{5}$$

Note that this version of the ME norm is proportional to the fourth power of the pressure field. As described by De Vries and Berkhout (1984), this $F(q_{k,l})$ is a strong entropy function, leading to a norm that primarily emphasises amplitude peaks. In other words, the fourth power enhances strong amplitudes and diminishes smaller ones. Consequently, a sparse, peaked amplitude distribution results in a high ME-norm value (i.e. the ME norm is maximised when entropy is minimised), whereas a dense, smooth distribution produces a lower ME-norm value. As illustrated in Fig. 1, ME-norm values decrease with increasing image density, confirming the effectiveness of such norm as a focusing metric.

While alternative convex entropy measures, such as Shannon or Kullback–Leibler entropy could be adopted, we employ the ME function defined by De Vries and Berkhout (1984) because of its sensitivity to focusing variations, which makes it particularly suitable for migration-based velocity estimation where localised diffraction focusing is the key diagnostic criterion.

2.2. Sensitivity analysis

To assess the ability of the ME norm to identify the optimal velocity model in terms of image focusing, we conducted a sensitivity analysis on a simple synthetic dataset. Fig. 2 displays the

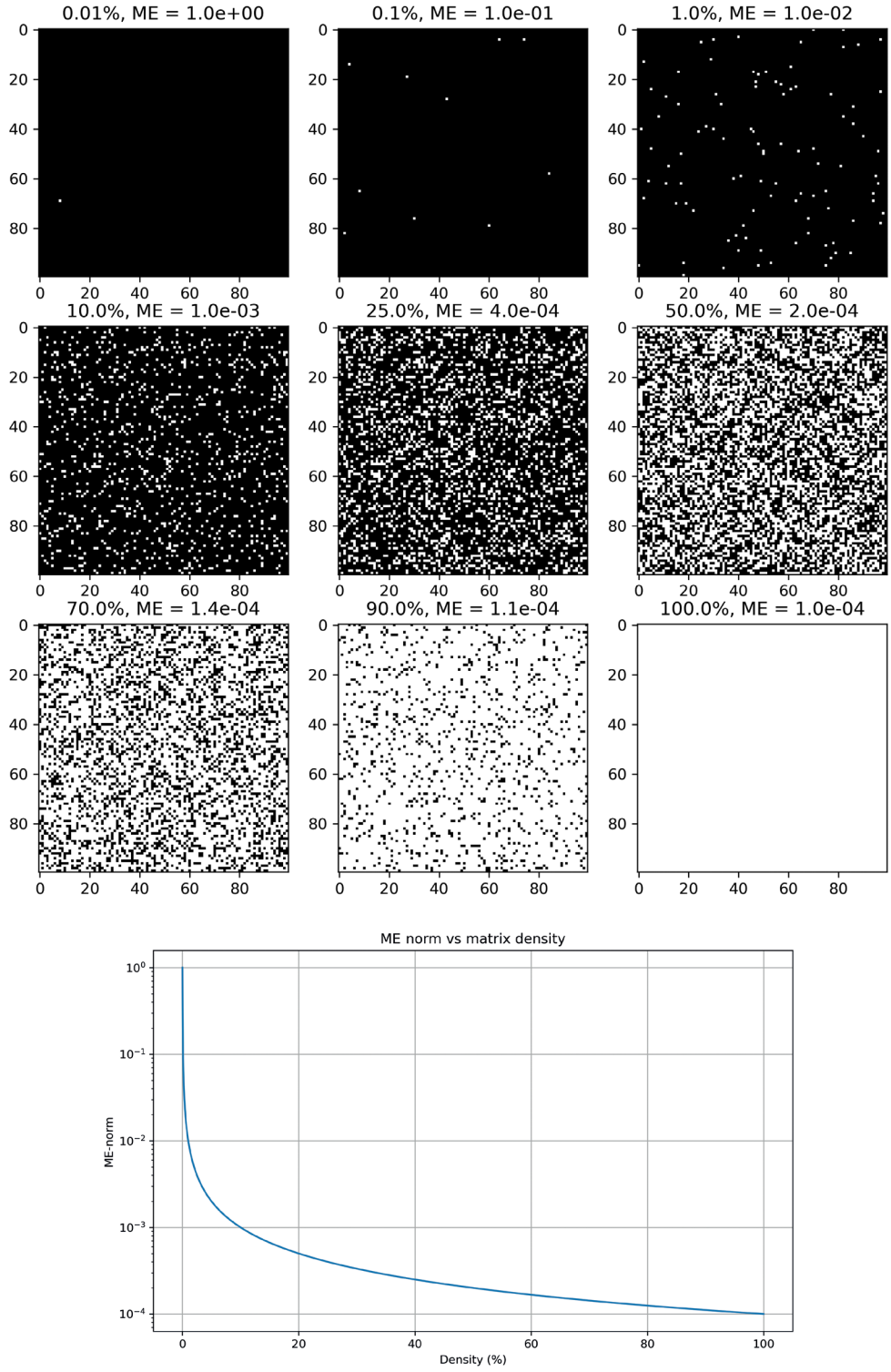

Fig. 1 - a) Nine matrices with increasing density, illustrating the relationship between matrix density and the ME norm. Each matrix is normalised so that the sum of its values equals 1. As the density of each matrix increases, a visual trend emerges: the ME norm decreases. b) Representation of the ME norm on the *y*-axis against the matrix density on the *x*-axis, demonstrating that greater matrix sparsity results in a higher ME-norm value.

velocity model (Fig. 2a) and the zero-offset dataset (Fig. 2b). The model consists of a uniform background velocity field and a spherical velocity anomaly to simulate diffraction from a finite-sized diffractor. The blue line shows the location of all the source-receiver pairs used to acquire the zero-offset dataset, while the red and light-blue rays illustrate the zero-offset wave propagation paths.

By considering the goal of adapting the ME norm as a cost function in a FWI algorithm, the RTM was run on this synthetic dataset using different velocity models and the ME norm was

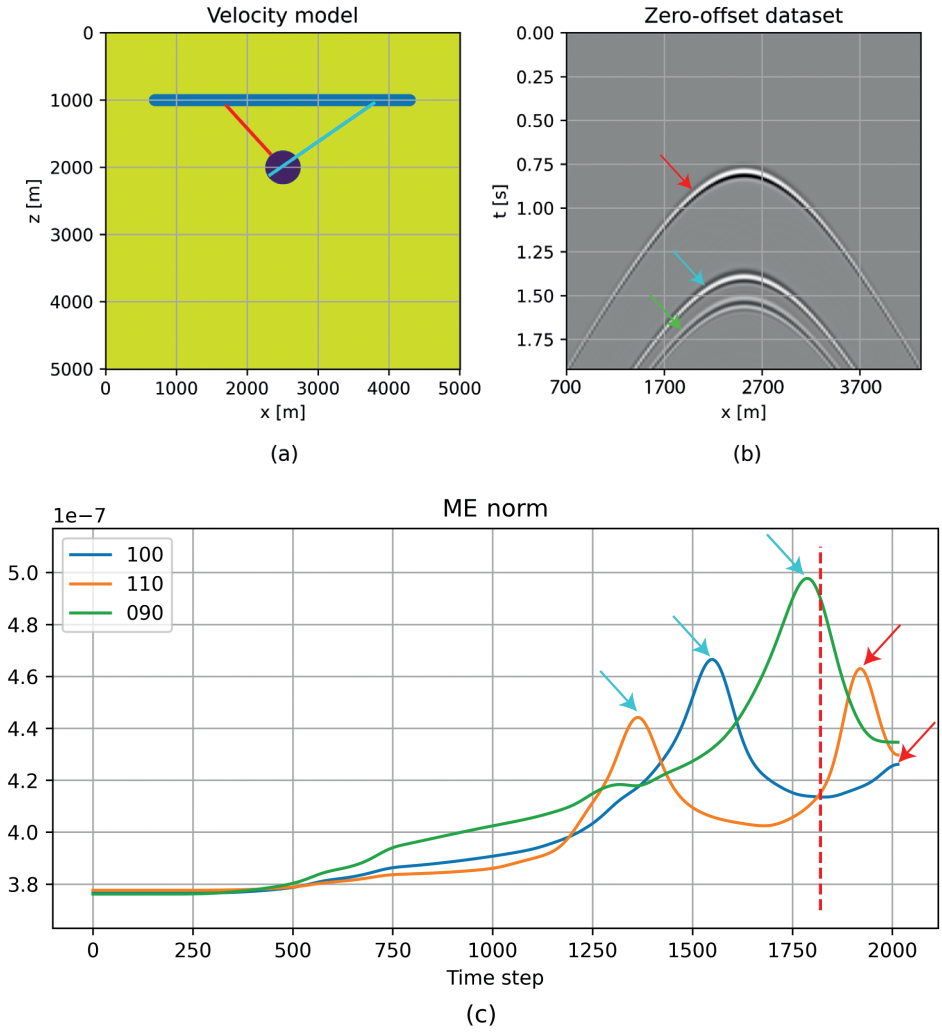

Fig. 2 - Synthetic dataset analysis. a) Uniform velocity model with a spherical anomaly. The blue line indicates the location of all the source-receiver pairs used to acquire the zero-offset dataset. The red and light-blue arrows show the zero-offset wave reflection from the convex feature and the concave feature, respectively. b) Zero-offset dataset. The red arrow shows the reflection caused by the upper convex discontinuity; the light-blue arrow points to the reflection from the lower concave discontinuity; the green arrow emphasises the refraction phenomena related to a lateral velocity discontinuity. c) The ME norm versus the time step computed after the RTM performed using the correct velocity (blue), 10% lower (green), and 10% higher (orange). The red arrows indicate the collapse of the reflection caused by the upper convex discontinuity; the light-blue arrows point to the collapse of the reflection from the lower concave discontinuity. The red dashed line marks the maximum acquisition time, emphasising that diffractions from convex and concave structures collapse at different times.

calculated at each time step. The various velocity models are generated by multiplying the original velocity model for a uniform scaling factor. Fig. 2c displays the ME norm as a function of the time step for the original velocity model (solid blue line), a 10% higher scaled velocity (solid orange line), and a 10% lower scaled velocity (solid green line). The ME-norm function showed ambiguity in cases where reflectors had significant curvature: when using the correct velocity, the maximum value of this function is reached before the maximum acquisition time (*T* marked by the dashed red line); when using the 10% lower velocity, a peak is observed near *T*. As previously noted by Biondi (2010), this effect arises from the inherent ambiguity between image focusing and the curvature of the reflector, causing diffractions from convex and concave structures to collapse at different times. These findings highlight that a cost function based on the ME norm is inadequate as it depends on the curvature of the reflectors. However, Fig. 2c also shows how the derivative of the ME norm effectively indicates the correct velocity at which the image reaches maximum focus. In fact, when the input velocity is correct, the ME norm approaches a horizontal tangent at time step *T*, which means the derivative of this quantity approaches zero.

2.3. Velocity update

Once established that the derivative of the ME norm effectively identifies the velocity that yields the optimal focus of an image, the mathematical expression of the cost function was formalised and the steepest-descent method was applied to update the velocity. In this method, the gradient of the cost function is calculated using the adjoint-state method (Plessix, 2006; Ren, 2022).

2.3.1. Cost function

The cost function (*J*) is defined in Eq. (6) as the squared difference of ME-norm values between adjacent time steps, summed over a time window centred at recording time *T*. This difference approximates the temporal derivative of the ME norm. The formula is expressed as follows:

$$J = \sum_{t=T-N}^{T+N} \{ \sum_{x,n} \left[ME\left(I_t(x,n,t)\right) - ME(I_t(x,n,t-1)) \right] \}^2 \tag{6}$$

where $ME(I_t(x, n, t))$ is the ME norm of the RTM output converted from depth to time $[I_t(x, n)]$ and weighted in time interval $t \in [T\text{-}N, T\text{+}N]$, with *T* being the recording time and *N* a fixed number of time steps. The time-window half-width *N* acts as a smoothing parameter in the temporal derivative of the ME norm. In this study, *N* was selected empirically by testing a range of values and evaluating the stability and sharpness of the resulting focusing curves. Too small an *N* made the derivative noisy, whereas overly large values smoothed out the focusing signature. The adopted *N* represents a compromise that ensured consistent image focusing for both the synthetic and field examples.

2.3.2. Adjoint-state method

The gradient of the cost function, $\partial J/\partial c$, is computed through the adjoint-state method (Plessix, 2006; Ren, 2022). This method finds the internal product between adjoint source $\partial J/\partial u$ and the derivative of the pressure field $u(x, z)$ with respect to velocity model $c(x, z)$, $\partial u/\partial c$. The mathematical formulation for calculating the gradient is as follows:

$$\frac{\partial J}{\partial c} = \left\langle \frac{\partial J}{\partial u}, \frac{\partial u}{\partial c} \right\rangle \tag{7}$$

where the adjoint-source is computed as the negative derivative of the cost function.

The velocity model is, then, updated as:

$$c_0 - \frac{\partial J}{\partial c}\delta c = c_1 \tag{8}$$

where c_0 is the input velocity, c_1 the updated velocity, and δc a velocity increment. We used a normalised, clipped version of the gradient to avoid numerical instabilities. The update procedure includes: a) gradient normalisation, b) clipping using a quantile-based interval, c) final normalisation, d) scaling by a fixed increment δc, e) model update via Eq. (8), f) RTM with the new velocity model c_1, g) conversion of the resulting image to time domain, h) ME-norm computation on the updated image.

The final image quality mainly depends on four factors: the initial velocity model, the chosen velocity increment, the acquisition geometry, and the structural complexity of the subsurface. Among these, the accuracy of the initial velocity model and the chosen velocity increment are the only controllable parameters affecting the convergence and the stability of the ME-norm-based update.

2.4. Field data test

The method was, then, applied to the Viking Graben Line 12 marine seismic dataset, acquired in the North Sea, between the UK and Norwegian sectors (Fig. 3). This dataset was originally used in the 1994 SEG Workshop on Comparison of Seismic Inversion Methods (Keys and Foster, 1998) and is publicly available on the SEG Wiki (SEG Wiki, 2021).

The Viking Graben is a geological feature that extends in a N-S direction known for its complex geology and significant hydrocarbon resources. For a detailed geological framework, see Keys and Foster (1998).

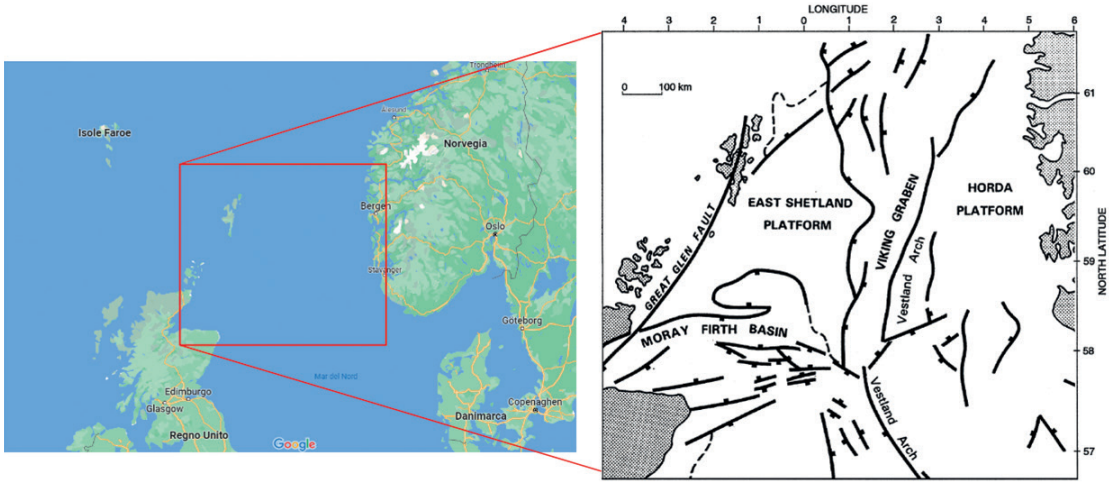

Fig. 3 - Map of the Viking Graben area (modified from Madiba and McMechan, 2003).

The dataset was collected in the northern region, with acquisition oriented along an E-W axis. This dataset comprises 1001 shots spaced 25 m apart. Each shot is recorded by 120 receivers, also spaced at 25 m, with offsets ranging from 262 to 3237 m. The maximum fold is 60 traces for a single common mid-point (CMP). Each trace contains 1500 samples with a sampling interval of 4 ms, resulting in a trace duration of 5.996 s.

The dataset underwent standard preprocessing (Fig. 4), including multiple suppression (not detailed here), CMP sorting, semblance analysis, normal moveout (NMO) correction, NMO muting, and stacking. The resulting interval velocity model (Fig. 5) and the corresponding stack (Fig. 6) were used as inputs for the ME-norm-based inversion.

Preprocessing steps such as CMP sorting, NMO correction, and stacking were performed in MATLAB using custom scripts. The RTM, ME-norm calculation, and velocity update were implemented in Python with a code written specifically for this work.

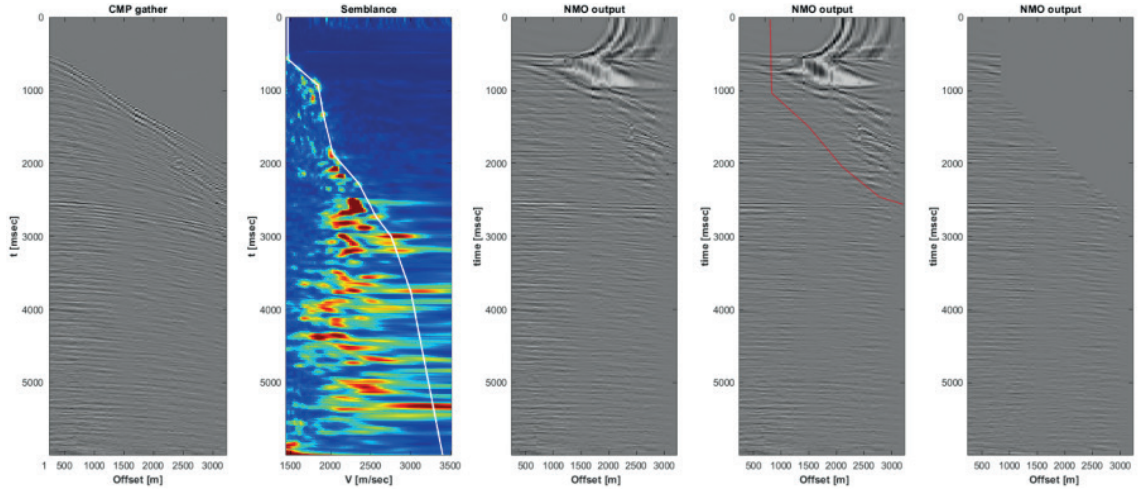

Fig. 4 - Workflow for a single CMP gather of the Viking Graben dataset: from left to right, CMP sorting, semblance analysis, NMO correction, NMO muting, NMO output.

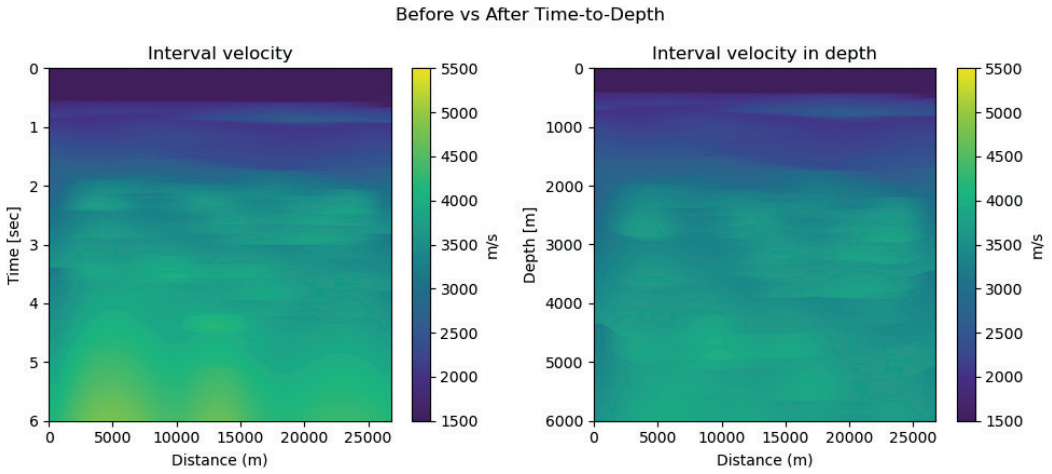

Fig. 5 - Viking Graben dataset line 12, processing results: interval velocity model.

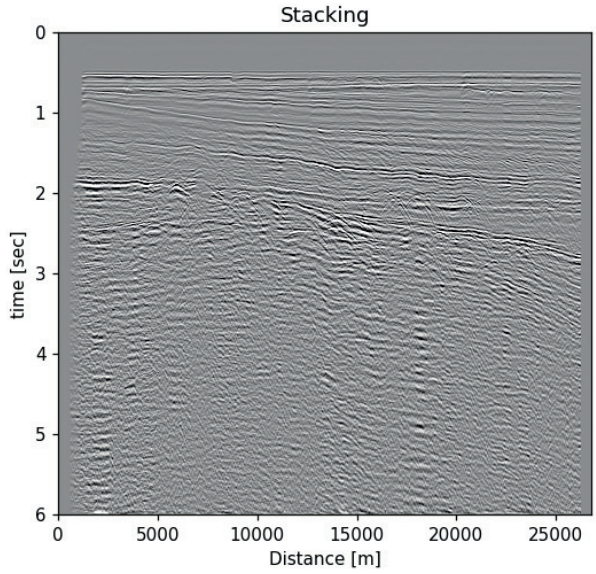

Fig. 6 - Viking Graben dataset line 12, processing results: stack section.

The stacked section (Fig. 6) and the corresponding interval velocity model highlight several key features of the dataset. The upper part of the section (above ~2 s two-way traveltime) is characterised by strong continuous reflections with moderate amplitude variation, indicating well-layered and laterally coherent structures. Below this depth, reflector continuity decreases and several dipping events appear, suggesting a more complex subsurface geometry with possible fault-related offsets. Some hyperbolic diffractions are also visible, mainly beneath high-contrast reflectors, revealing small-scale heterogeneities and lateral velocity variations. The velocity model shows an increase with depth, consistent with compaction trends, but also local lateral variations. Multiple reflections and diffractions are evident and these features influence image focusing. The dataset, therefore, provides a suitable test case for evaluating the ME-norm-based approach.

3. Results and discussion

The proposed method was applied to the Viking Graben dataset to assess its performance (Fig. 7). The original image in Fig. 7a was obtained by applying post-stack RTM using the initial velocity model derived from the semblance analysis. The updated image in Fig. 7b was produced with the velocity model obtained after a single velocity-update step driven by the ME-norm-based cost function.

Velocity increment δc was selected considering the nonlinear nature of the inversion problem. Since the gradient of the cost function provides a valid search direction only for small perturbations of the velocity model, larger updates could violate the linear approximation assumed in the steepest-descent method. Therefore, a 30 m/s increment was adopted to maintain the validity of the linear approximation and to ensure a stable and interpretable image update.

To better demonstrate the improvements, two zoomed-in areas are also displayed. In these regions, improved reflector continuity and increased contrast are evident.

These results suggest that a cost function based on the derivative of the ME norm can be effectively incorporated into the FWI framework. The observed improvements in image focusing

support the viability of this approach. Although the current implementation is preliminary, the positive outcomes encourage further development. We believe that with additional refinement, a fully operational FWI algorithm, driven by image focusing, can be realised, offering a viable alternative for seismic imaging in contexts with offset or fold limitations which are conditions often encountered in vintage datasets.

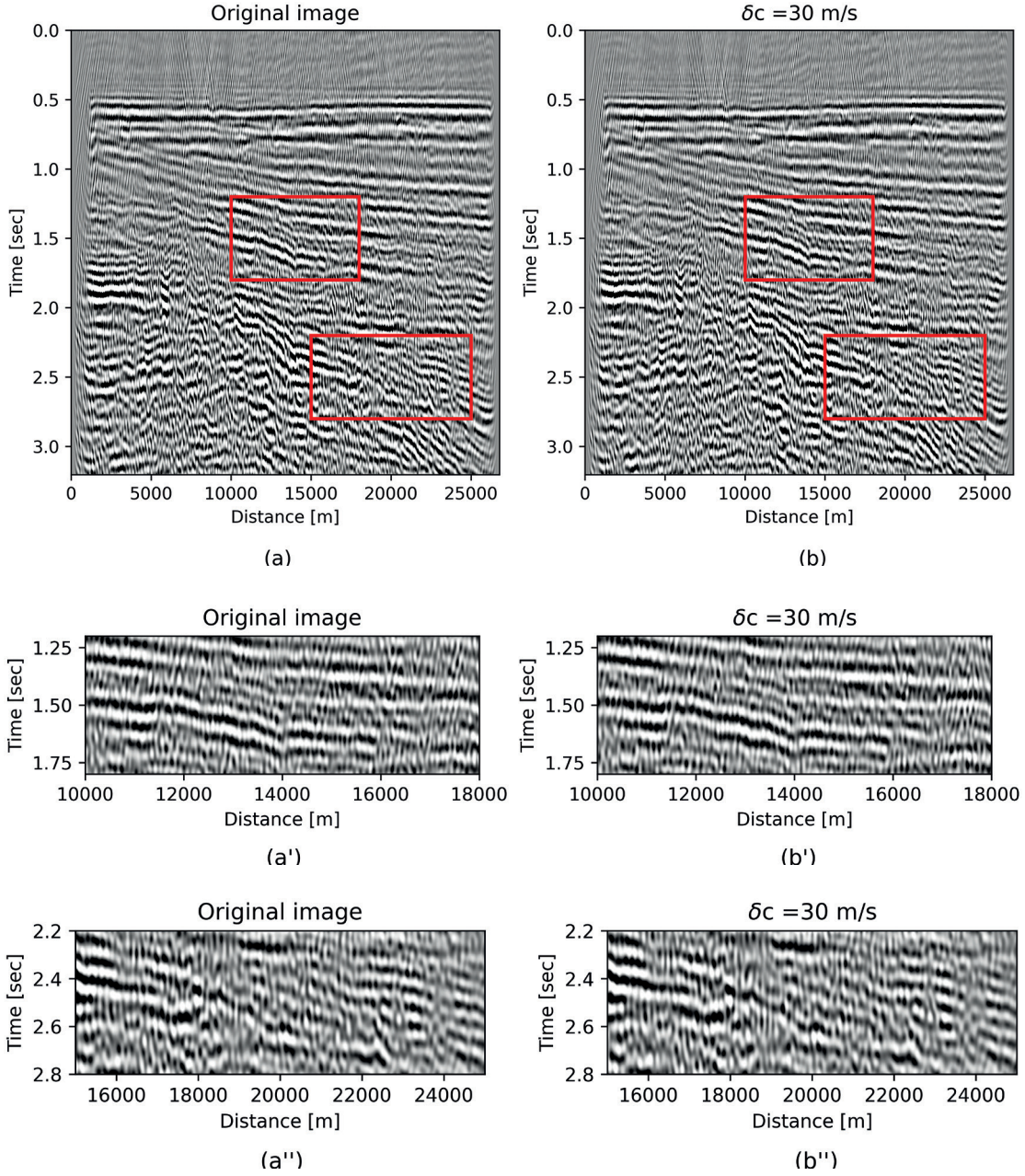

Fig. 7 - Comparison between the original image (obtained using the initial velocity in the RTM algorithm) and the image after the velocity update with a velocity increment δc = 30 m/s (panels a and b). Comparisons referred to specific areas (panels a', b' and a'', b''). Clearer alignment and higher contrast are visible in the images after the velocity update suggesting that implementing a FWI algorithm driven by image focusing is feasible.

Fig. 8 compares the initial velocity model with the difference map after one ME-norm-based update. The most significant velocity variations occur in the shallower part of the section (upper red box), where diffractions provide a clearer focusing response. In this zone, the updated image exhibits improved reflector alignment and sharper amplitude definition. In contrast, the deeper interval (lower red box) shows only minor velocity changes (< 10 m/s), consistent with the lower diffraction density and reduced sensitivity of the ME-norm derivative at greater travel times. Consequently, the visual improvement in the deeper region is more subtle, reflecting the limited focusing information available from the data at such depths.

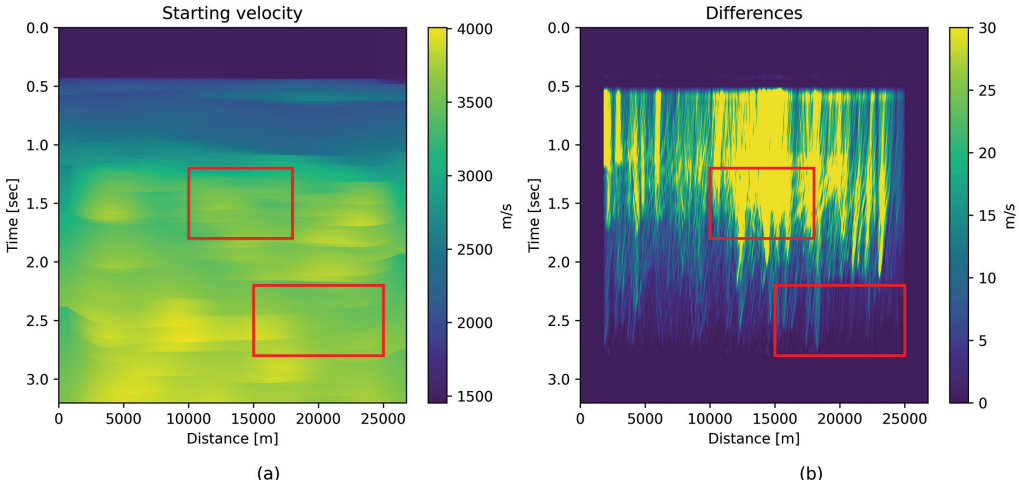

Fig. 8 - a) Initial velocity model; b) velocity differences after one ME-norm-based update. Red boxes highlight the shallow and deep regions discussed in the text.

Similar diffraction-based approaches have been proposed in recent years, confirming the potential of image focusing for velocity estimation from limited-offset data. These studies, although based on different implementations, all support the conclusion that diffraction-focused analysis provides reliable velocity information where conventional moveout-based methods are limited, consistent with the findings of this work.

4. Conclusions

This study highlights the potential of the ME norm in identifying optimal velocity models and driving velocity updates using the adjoint-state method. The derivative of the ME norm effectively indicates image focusing quality and, when incorporated into a cost function, provides meaningful model updates within a FWI framework.

The proposed approach was first assessed on a synthetic dataset to validate the sensitivity of the ME-norm derivative to velocity variations and to confirm its effectiveness as a focusing-based cost function. The method was, then, applied to the Viking Graben Line 12 dataset (North Sea). The results show that the most significant velocity variations occur in the shallower part of the section, where diffractions are more evident and focusing information is stronger. These updates lead to improved reflector continuity and contrast in the migrated image.

The final image quality was found to depend mainly on the initial velocity model, the presence of diffractions, the acquisition geometry, and the structural complexity of the subsurface.

While this work represents a single-step proof of concept, it establishes the feasibility of using image focusing as a robust cost function within FWI workflows. The method shows potential for improving seismic imaging from post-stack data, especially in situations with limited acquisition geometry, where fold or offset are small, such as those typical of offshore wind farm surveys and geological storage monitoring. Ultimately, this approach provides a cost-effective and computationally efficient solution for enhanced subsurface characterisation.

Acknowledgments. This paper is based on work carried out by E. Ligas during her Master's thesis and was presented at the GNGTS 2025, Bologna, Italy. We gratefully acknowledge the support of the International Cooperation Program WATER4ALL 2022 – the RESCUE Project.

REFERENCES

Baysal E., Kosloff D. and Sherwood J.; 1983: *Reverse time migration.* Geophys., 48, 1514-1524, doi: 10.1190/1.1441434.

Biondi B.; 2010: *Velocity estimation by image-focusing analysis.* Geophys., 75, U49-U60, doi: 10.1190/1.3506505.

De Vries D. and Berkhout A.J.; 1984: *Velocity analysis based on minimum entropy.* Geophys., 49, 2132-2142, doi: 10.1190/1.1441629.

Fomel S., Landa E. and Taner M.T.; 2007: *Poststack velocity analysis by separation and imaging of seismic diffractions*. Geophys., 72, U89-U94, doi: 10.1190/1.2781533.

Keys R.G. and Foster D.J.; 1998: *Comparison of seismic inversion methods on a single real data set*. Soc. Explor. Geophys., 213 pp., doi: 10.1190/1.9781560802082.

Madiba G.B. and McMechan G.A.; 2003: *Processing, inversion, and interpretation of a 2D seismic data set from the North Viking graben, North Sea.* Geophys., 68, 1408-1422, doi: 10.1190/1.1581036.

Nasif A.; 2024: *Optimal processing of single-channel sparker marine seismic data.* Acta Geophys., 73, 421-437, doi: 10.1007/s11600-024-01403-6.

Plessix R.E.; 2006: *A review of the adjoint-state method for computing the gradient of a functional with geophysical applications.* Geophys. J. Int., 167, 495-503, doi: 10.1111/j.1365-246X.2006.02978.x.

Preine J., Schwarz B., Bauer A. and Hübscher C.; 2020: *When there is no offset: a demonstration of seismic diffraction imaging and depth-velocity model building in the southern Aegean Sea.* J. Geophys. Res.: Solid Earth, 125, e2020JB019961, doi: 10.1029/2020JB019961.

Ren Q.; 2022: *Seismic acoustic full waveform inversion based on the steepest descent method and simple linear regression analysis.* J. Appl. Geophys., 203, 104686, doi: 10.1016/j.jappgeo.2022.104686.

Santos L.A., Neves E., Freire F., Cetale Santos M.A., Matsumoto R. and Ajus Hide C.M.I.; 2020: *Diffraction velocity analysis in a single-channel seismic survey in the Joetsu basin.* Geophys., 85, U47-U53, doi: 10.1190/geo2019-0011.1.

SEG Wiki; 2021: *Mobil AVO Viking graben line 12.* <wiki.seg.org/wiki/Mobil_AVO_viking_graben_line_12>.

Weibull W. and Arntsen B.; 2014: *Reverse-time demigration using the extended-imaging condition*. Geophys., 79, WA97-WA105, doi: 10.1190/geo2013-0232.1.

Whitmore N.D.; 1983: *Iterative depth migration by backward time propagation.* SEG Tech. Program Expanded Abstracts, pp. 382-385, doi: 10.1190/1.1893867.

Corresponding author: Elisa Ligas
Department of Mathematics, Informatics and Geosciences, University of Trieste
Via Edoardo Weiss 1, 34128 Trieste, Italy
Phone: +39 345 1113313; e-mail: elisa.ligas@phd.units.it